Available online at www.sciencedirect.com
ScienceDirect
Journal of the European Ceramic Society 31 (2011) 291–298
www.elsevier.com/locate/jeurceramsoc

# $TiO_2$, $TiO_2$/Ag and $TiO_2$/Au photocatalysts prepared by spray pyrolysis

Astri Bjørnetun Haugen [a,*], Izumi Kumakiri [b], Christian Simon [b], Mari-Ann Einarsrud [a]

[a] *Department of Materials Science and Engineering, Norwegian University of Science and Technology, N-7491 Trondheim, Norway*
[b] *SINTEF Materials and Chemistry, P.O. Box 124 Blindern, N-0314 Oslo, Norway*

Received 5 July 2010; received in revised form 23 September 2010; accepted 2 October 2010
Available online 29 October 2010

**Abstract**

$TiO_2$, $TiO_2$/Ag and $TiO_2$/Au photocatalysts exhibiting a hollow spherical morphology were prepared by spray pyrolysis of aqueous solutions of titanium citrate complex and titanium oxalate precursors in one-step. Effects of precursor concentration and spray pyrolysis temperature were investigated. By subsequent heat treatment, photocatalysts with phase compositions from 10 to 100% rutile and crystallite sizes from 12 to 120 nm were obtained. A correlation between precursor concentration and size of the hollow spherical agglomerates obtained during spray pyrolysis was established. The anatase to rutile transformation was enhanced with metal incorporations and increased precursor concentration. The photocatalytic activity was evaluated by oxidation of methylene blue under UV-irradiation. As-prepared $TiO_2$ particles with large amounts of amorphous phase and organic residuals showed similar photocatalytic activity as the commercial Degussa P25. The metal incorporated samples showed comparable photocatalytic activity to the pure $TiO_2$ photocatalysts.


*Keywords:* Spray pyrolysis; $TiO_2$; Photocatalysis

## 1. Introduction

The photocatalytic properties of $TiO_2$, as discovered by Fujishima and Honda, have been utilized for decades in applications such as self-cleaning windows and anti-bacterial coatings.[1,2] Oxidation of natural organic matters (NOM) and pesticides in ground water is another possible application of $TiO_2$-photocatalysis.[3,4] By UV-irradiation, these organic compounds are oxidized into their corresponding mineral acids, $CO_2$ and $H_2O$ by radical mechanisms.[5] The pure anatase phase of $TiO_2$ is more photoactive than the pure rutile phase due to higher oxygen vacancy concentration.[6] However, a synergy effect due to either the rutile phase acting as an electron sink or rutile extending the photoactivity into the visible light range leads to enhanced photocatalytic activity of a mixture of both phases.[7] A phase composition of ~30% rutile and 70% anatase is reported as the optimum.[8] Exact mechanism of photocatalysis is not agreed upon, although hydroxide groups on the surface with trapped holes are generally accepted to be of importance.[5] A large specific surface area is generally favourable in catalysis. For $TiO_2$ photocatalysts, an additional improvement is found for nanoparticles <5 nm, due to quantum size effects,[5] and for hollow structures.[9,10]

Recombination of electrons and holes is a significant loss mechanism during photocatalysis in $TiO_2$.[11] Large crystallite sizes reduce recombination at grain boundaries.[12] Metal deposits can facilitate transfer of excited electrons to a metal particle and trap them in a Schottky barrier,[11] hence increased photocatalytic activity is found for incorporations such as Ag,[13–15] Au,[16–20] Pd[17] and Pt.[17,21]

For photocatalytic studies the commercial photocatalyst P25[7,8,22] from Evonik Degussa is usually employed, either unmodified or as a starting material for metal deposited $TiO_2$.[17,19] $TiO_2$ photocatalysts have also been prepared by sol–gel routes,[13,15,23,24] by use of colloidal $TiO_2$[11] and solvothermal methods.[25] However, for preparation of larger volumes, spray pyrolysis is a promising method which also permits synthesis of hollow spheres[26] with potential application within encapsulation.[27] A range of precursors (Ti-isopropoxide in non-aqueous solutions,[5,16,28,29] colloidal $TiO_2$ suspensions and titanyl sulphate in sulphuric acid[30]) and techniques[16,18,31,32] has been utilized for manufacture of various $TiO_2$-systems.[29,32,33]

* Corresponding author.
*E-mail address:* mari-ann.einarsrud@material.ntnu.no (A.B. Haugen).

0955-2219/$ – see front matter © 2010 Elsevier Ltd. All rights reserved.
doi:10.1016/j.jeurceramsoc.2010.10.006

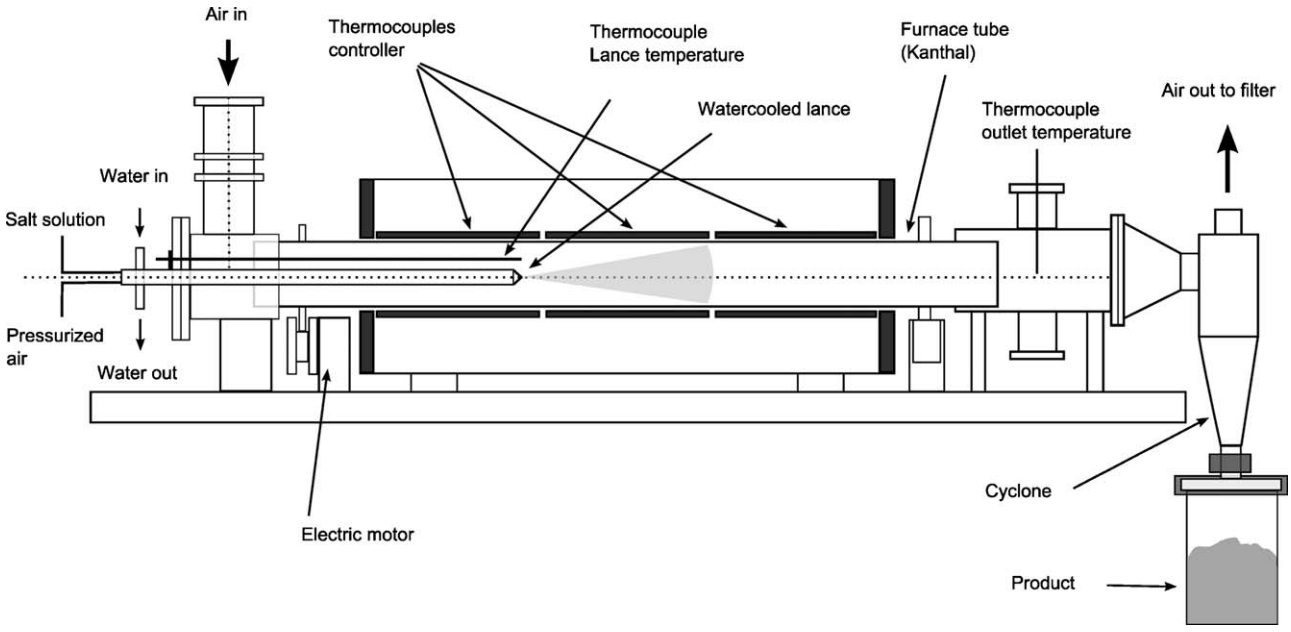


Fig. 1. Schematic overview of the spray pyrolysis equipment.

This study presents synthesis of $TiO_2$, $TiO_2$/Ag and $TiO_2$/Au photocatalysts by spray pyrolysis of aqueous solutions of titanium citrate complex and titanium oxalate. The emphasis has been on process modifications to obtain photocatalysts with high activity as well as the production of particles with a designed morphology.

## 2. Experimental

### 2.1. Powder preparation

The Ti–citrate complex precursors were prepared by adding titanium(IV) isopropoxide (AlfaAesar, 97+%) to a solution of

Table 1
Sample codes, precursor type, precursor concentration, set temperature and type and amount of metal incorporation for the different spray pyrolysed $TiO_2$ photocatalysts grouped in series according to varied parameters.

| Series/sample code | Precursor | Precursor concentration (M) | Set temperature (°C) | Ag (wt%) | Au (wt%) |
|---|---|---|---|---|---|
| *Precursor series* | | | | | |
| Ti–oxalate | Ti–oxalate | 0.25 | 1000 | 0 | 0 |
| Ti–citrate | Ti–citrate | 0.5 | 1000 | 0 | 0 |
| *Temperature series* | | | | | |
| 1000 °C | Ti–citrate | 0.5 | 1000 | 0 | 0 |
| 875 °C | Ti–citrate | 0.5 | 875 | 0 | 0 |
| 850 °C | Ti–citrate | 0.5 | 850 | 0 | 0 |
| 825 °C | Ti–citrate | 0.5 | 825 | 0 | 0 |
| 800 °C | Ti–citrate | 0.5 | 800 | 0 | 0 |
| *Ag series* | | | | | |
| 0% Ag | Ti–citrate | 0.5 | 800 | 0 | 0 |
| 6.5% Ag | Ti–citrate | 0.5 | 800 | 6.5 | 0 |
| 10.6% Ag | Ti–citrate | 0.5 | 800 | 10.6 | 0 |
| *Au series* | | | | | |
| 0% Au | Ti–citrate | 0.5 | 800 | 0 | 0 |
| 0.24% Au | Ti–citrate | 0.5 | 800 | 0 | 0.24 |
| 1% Au | Ti–citrate | 0.5 | 800 | 0 | 1 |
| 3% Au | Ti–citrate | 0.5 | 800 | 0 | 3 |
| *Concentration series* | | | | | |
| 0.6 M | Ti–citrate | 0.6 | 800 | 0 | 0 |
| 0.5 M | Ti–citrate | 0.5 | 800 | 0 | 0 |
| 0.3 M | Ti–citrate | 0.3 | 800 | 0 | 0 |
| 0.15 M | Ti–citrate | 0.15 | 800 | 0 | 0 |
| 0.06 M | Ti–citrate | 0.06 | 800 | 0 | 0 |

Table 2
Specific surface area, amount of rutile and rutile and anatase crystallite sizes of the different as-prepared spray pyrolysed $TiO_2$ photocatalysts.

| Series/Sample code | Specific surface area ($m^2$/g) ±4% | Amount of rutile (wt%) ±6% | Rutile size (nm) ±6% | Anatase size (nm) ±6% |
|---|---|---|---|---|
| *Precursor series* | | | | |
| Ti–oxalate | 94 | 35 | 80 | 13 |
| Ti–citrate | 33 | 89 | 46 | 12 |
| *Temperature series* | | | | |
| 1000 °C | 33 | 89 | 46 | 12 |
| 875 °C | 27 | 48 | 25 | 8 |
| 850 °C | 22 | 53 | 39 | 8 |
| 825 °C | 26 | 57 | 25 | 7 |
| 800 °C | 30 | 70 | 38 | 16 |
| *Ag series* | | | | |
| 0% Ag | 30 | 70 | 38 | 16 |
| 6.5% Ag | 25 | Amorphous | Amorphous | Amorphous |
| 10.6% Ag | 24 | Amorphous | Amorphous | Amorphous |
| *Au series* | | | | |
| 0% Au | 30 | 70 | 38 | 16 |
| 0.24% Au | 26 | 68 | 24 | 13 |
| 1% Au | 32 | 75 | 43 | 19 |
| 3% Au | 29 | 68 | 23 | 9 |
| *Concentration series* | | | | |
| 0.6 M | 26 | 63 | 31 | 12 |
| 0.5 M | 30 | 70 | 38 | 16 |
| 0.3 M | 35 | 63 | 33 | 15 |
| 0.15 M | 42 | 80 | 55 | 17 |
| 0.06 M | 48 | 67 | 52 | 21 |

citric acid (Sigma–Aldrich, 99.0+%) in distilled water with a molar ratio of 1:3 of Ti-isopropoxide to citric acid. During addition of Ti-isopropoxide, the citric acid solution was kept at ∼90 °C at vigorous stirring while nitrogen gas was flushed over the system. The resulting Ti–citric acid complex solution was then diluted to the desired concentration (0.6–0.06 M) and left stirring at ∼70 °C for 12 h to obtain a clear solution, which was filtered and thermogravimetrically standardized. For the metal incorporated precursors, gold chloride trihydrate (Sigma–Aldrich, ACS reagent) or silver acetate (AlfaAesar, 99%) was dissolved in parts of the 0.5 M Ti–citrate complex solution under reduced exposure to light. A 0.25 M precursor solution was obtained by dissolving titanium oxalate (Pfaltz & Bauer, 99%) in water at 70 °C, then left stirring for 12 h and filtered.

The precursor solutions were atomized by a two-phase nozzle with internal mixing of liquid and pressurized air (150 kPa) into a furnace. Estimated range of droplet size is 20–40 μm. Set temperature of the furnace was in the range 800–1000 °C, temperature at the nozzle was measured to be ∼150 °C below the set temperature. Residence time calculated from the air flow through the system is 0.4 s. A schematic of the furnace is given in Fig. 1. An overview of the precursors employed and operation temperatures is shown in Table 1, listed in series according to the parameters varied. The as-prepared powders were calcined for 3 h at temperatures ranging from 550 to 900 °C to alter the phase composition and crystallite size. The heating and cooling rates were ∼200 °C/h.

### 2.2. Powder characterization

As-prepared and calcined powders were characterized by Cu Kα X-ray diffraction in a Bruker AXS D8Focus (slit size 0.2, range 20–50° 2$\theta$, step size 0.03° 2$\theta$ and step time 1–3 s). Phase

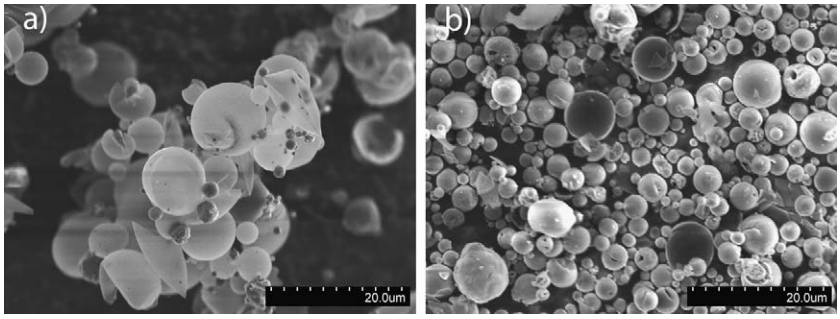


Fig. 2. Scanning electron micrographs of hollow spheres of $TiO_2$ photocatalyst as-prepared by spray pyrolysis. (a) Powders prepared from 0.5 M Ti–citrate solution, and (b) powders prepared from 0.06 M Ti–citrate solution.

composition of the samples was calculated from the intensities of the diffraction lines by the Spurr equation[34] and the average crystallite sizes were calculated by the Scherrer equation.[15] Small amounts of selected powders were sprinkled on a carbon tape and inspected by SEM (Hitachi S-3400N LV-SEM). Diameter and shell thicknesses were measured as the average of 50 of the intact and 10 of the broken hollow spheres, respectively. The Brunauer–Emmett–Teller (BET) specific surface area of selected powders was measured by nitrogen adsorption on a Micromeritics TriStar 3000 after degassing at 250 °C for ~12 h in vacuum. TEM analyses were carried out on a JEM-2010 equipped with EDS (Oxford Instruments) for element detection. The powders were dispersed in acetone or 100% ethanol and supported on a holey carbon Cu-grid.

### 2.3. Photocatalytic oxidation tests

The Ag- and Au-incorporated samples, as well as pure $TiO_2$ samples from alkoxide and oxalate precursors were selected for photocatalytic testing along with Degussa P25.[7,8,22] The photocatalysts (~2 mg) were soaked in 1 ml of methylene blue solutions (Sigma–Aldrich) and left in the dark for more than 12 h. Portions (260 μl) of these methylene blue solutions were then investigated in a UV–vis spectrophotometer (PowerWave XS BioTek). Conversion from absorption to concentration data was performed automatically based on calibration from solutions with known methylene blue concentration over a large concentration range. After transferring the liquid portions back to the photocatalysts, UV-light (3 black lamps irradiating at ~350 nm, each 8 W, 300 μW measured at sample spot) was applied for 5 min before the concentration was re-measured. Successive UV-irradiation and concentration measurements were applied up to a total irradiation time of 90 min. Methylene blue solutions without any catalysts were treated under the same conditions as references.

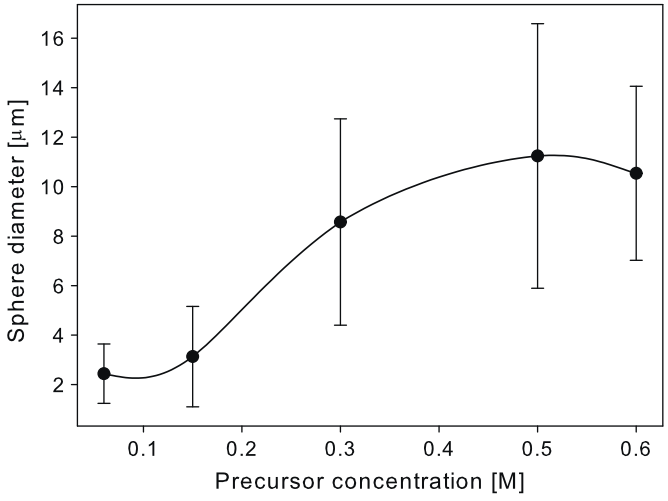


Fig. 3. Diameter and shell thickness of hollow $TiO_2$ spheres prepared by spray pyrolysis of Ti–citrate solution vs. Ti–citrate concentration. Lines are guides to the eyes.

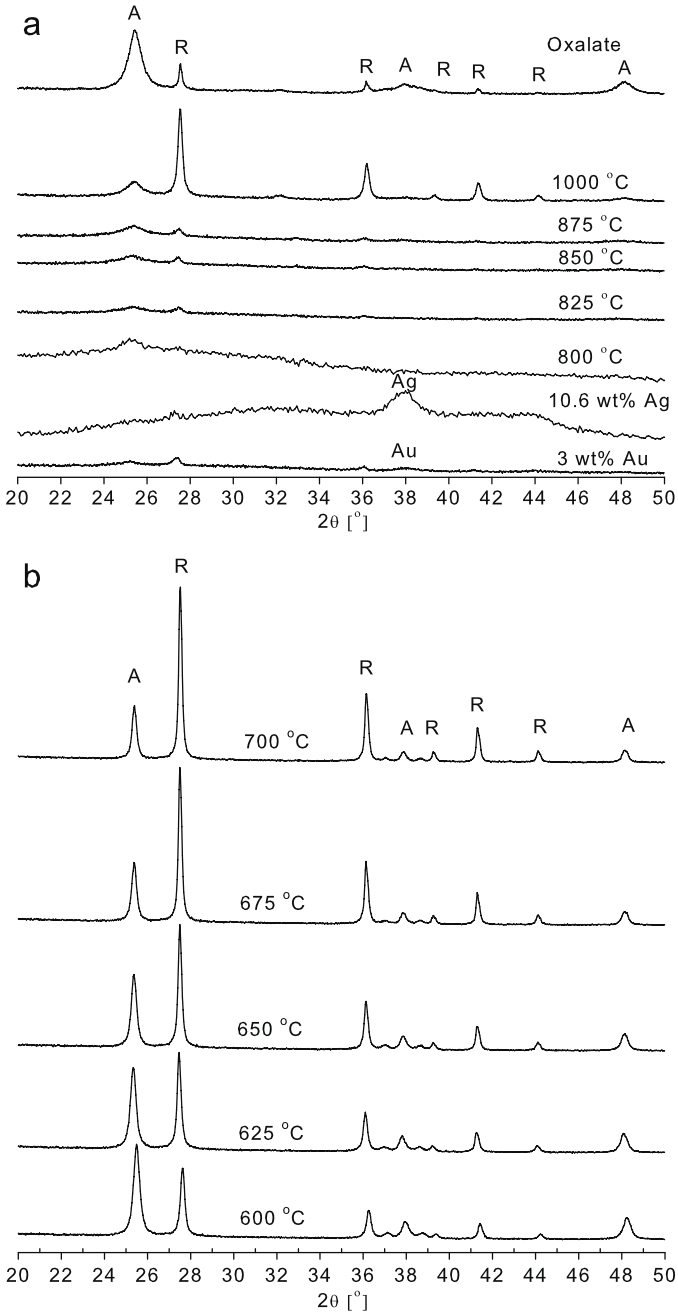


Fig. 4. (a) XRD-patterns of selected as-prepared $TiO_2$ photocatalysts prepared by spray pyrolysis. (b) Typical development of XRD-patterns of $TiO_2$ photocatalyst calcined at different temperatures, here shown by sample 0.5 M in the concentration series.

## 3. Results and discussion

### 3.1. Properties of as-prepared powders

Table 2 lists specific surface area, amount of rutile of the crystalline phase, and rutile and anatase crystallite sizes of all as-prepared powders obtained by spray pyrolysis. The specific surface area of the as-prepared powders was in the range 22–48 $m^2/g$ with an exception of the powder from the oxalate precursor where a specific surface area of 94 $m^2/g$ was obtained

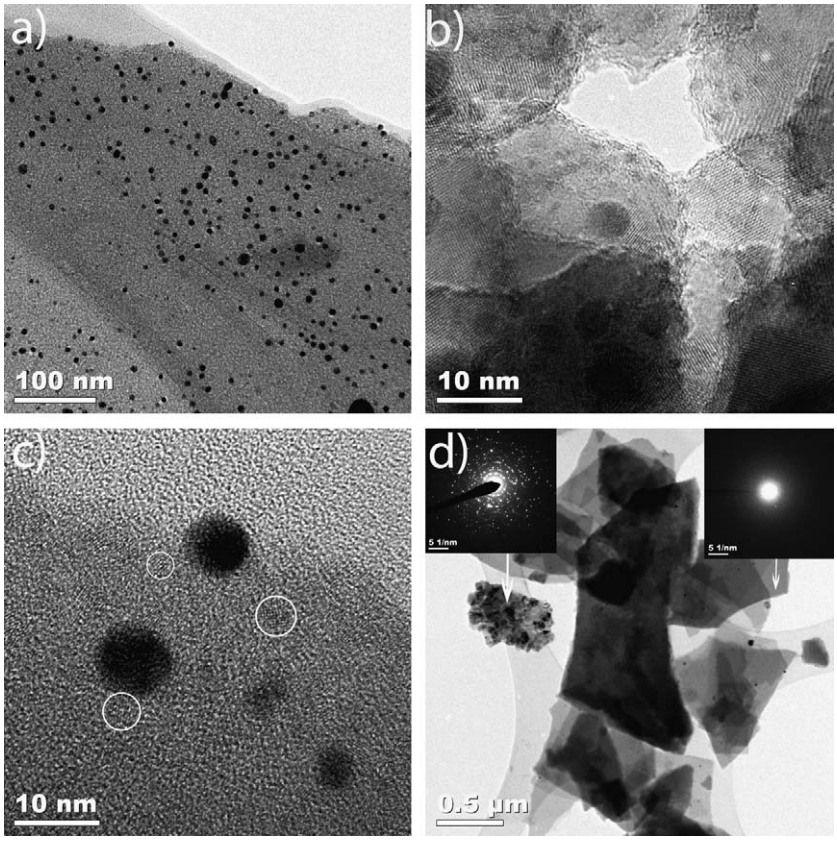


Fig. 5. Transmission electron micrographs of spray pyrolysed $TiO_2$ photocatalysts. (a) As-prepared $TiO_2$ with 3 wt% Au, showing evenly distributed Au particles (dark spots), (b) $TiO_2$ with 10.6 wt% Ag calcined at 625 °C, (c) crystalline and amorphous areas of as-prepared $TiO_2$ powder with 3 wt% Au, white circles indicate some of the crystalline areas indexed to anatase, and (d) crystalline and amorphous areas of as-prepared $TiO_2$ with 3 wt% Au, inserts are electron diffraction patterns.

(Table 2). Larger specific surface areas were obtained from lower precursor concentrations.

Fig. 2 shows the hollow spherical morphology exhibited by all the as-prepared powders due to the atomization–evaporation sequence taking place during the spray pyrolysis. By comparing the micrographs in Fig. 2a and b, a significantly smaller sphere size for the lower precursor concentration can be observed. In Fig. 3 the decrease in sphere size is plotted as a function of precursor concentration. The decrease in size is ascribed to increased shrinkage of the droplets during the drying step, since the initial droplet size was fixed. A decrease in shell thickness is also observed with decreasing shell size, based on measurements on broken shells. Variation in use of titanium precursor (Ti–citrate or Ti–oxalate), metal incorporation or preparation temperature did not produce any significant change in morphology.

In Fig. 4a, the XRD-patterns for as-prepared powders are shown. Differences in phase composition can be observed as intensity differences of the anatase and rutile diffraction lines. The powders were observed to be mostly amorphous at set temperatures lower than 1000 °C. The fraction of rutile relative to anatase phase was decreasing with increasing set temperatures from 825 to 875 °C (Table 2). As anatase is the metastable low-temperature phase, more rutile is expected at higher temperatures. The short residence time for the powder in the spray pyrolysis furnace could explain the large amount of amorphous $TiO_2$ and the unexpected phase distribution of the crystalline $TiO_2$ within this temperature region.

The powders sprayed at a set temperature of 1000 °C differ with respect to phase composition; the Ti–oxalate precursor gave 35 wt% rutile, while the Ti–citrate precursor yielded powder with 89 wt% rutile (Table 2 and Fig. 4a). The real preparation temperature experienced by the powder is as mentioned always lower than the set temperature of the furnace, in addition it is affected by the chemical reactions occurring in the atomized solution. By using the Ti–citrate precursor an exothermic combustion occurs in the formed hollow spheres and the real temperature is suggested to be significantly higher than during the endothermic decomposition of the Ti–oxalate solution. This explains the larger amount of rutile in the powder prepared from Ti–citrate than from Ti–oxalate.

Diffraction lines of Ag or Au were observed in the XRD-patterns of the samples containing these metals (Fig. 4a). This confirms that Ag and Au ions are thermally reduced during the spray pyrolysis process and are present as metal rather than ionic dopants in the $TiO_2$ structure. The diffraction lines for Ag or Au were observed for 3 wt% Au and 6.5 and 10.6 wt% Ag, while lower metal loadings were not detectable by XRD. The average metal crystallite sizes measured by XRD were 7, 9 and 19 nm for 10.6 wt% Ag, 6.5 wt% Ag and 3 wt% Au, respectively.

TEM investigations (Fig. 5) show the Au and the Ag nanoparticles (dark spherical dots) in the $TiO_2$-matrix (brighter). As seen

from Fig. 5a, the metal nanoparticles are evenly distributed. The size of these nanoparticles as found by TEM are ∼5 nm for Ag calcined at 625 °C (Fig. 5b), ∼10–15 nm for Au in the as-prepared sample (Fig. 5c) and 20–30 nm when calcined at 600 °C (micrograph not included). Larger surface mobility of Au compared to Ag could explain the larger size of the Au particles in the calcined samples. The presence of Au or Ag was also confirmed by EDS (not included).

By closer examination of the amorphous region in Fig. 5c lattice fringes indexed as anatase were found within the amorphous $TiO_2$ region. Furthermore, TEM-investigation with selected area electron diffraction (Fig. 5d) showed that the as-prepared powders consisted of amorphous flakes and crystalline agglomerates. By XRD, the crystalline part of this sample was found to contain 68 wt% rutile. As no rutile was observed within the amorphous regions, it is proposed that rutile may form directly during the spray pyrolysis process in separate agglomerates, while anatase is nucleated within the amorphous regions and grows during further heat treatment. Since the rutile fraction was decreasing with set temperature increasing from 825 to 875 °C, it is suggested that the larger amount of anatase formed at higher temperatures is due to increased growth of the anatase nuclei inside the amorphous regions.

### 3.2. Effect of calcination

An example of the typical evaluation of XRD-patterns with increasing calcination temperature is shown in Fig. 4b. Diffraction lines corresponding to rutile become more intense while the anatase lines are less intense as the calcination temperature is increased. Phase composition for several of the samples is plotted as a function of calcination temperature in Fig. 6 which shows that for all the samples the fraction of rutile increases with increasing calcination temperature. Decreased fraction of rutile relative to anatase with respect to the as-prepared powder can be observed for some samples due to a large amount of amorphous $TiO_2$ (undetected by XRD) transforming to anatase. For samples containing Ag (Fig. 6a), an accelerated transformation to rutile compared to the pure $TiO_2$ powder was observed in accordance with previous studies.[15] A similar effect, contradicting previous studies[24] was found for the Au-incorporated powders (Fig. 6b) and for the samples from the more concentrated precursors (0.6–0.3 M) compared to the more diluted (0.15–0.06 M) (Fig. 6c). The microstructure of the hollow spherical agglomerates was maintained upon calcination.

Coarsening of anatase and rutile crystallites during calcination is shown in Fig. 7. Anatase crystallite sizes increased to ∼50 nm, rutile to ∼80 nm at 700 °C. Since the phase transformation from anatase to rutile occurred simultaneously, the crystallite sizes and phase composition are coupled; this is especially clear for the anatase crystallite sizes of powders from different precursor concentrations.

### 3.3. Photocatalytic evaluation results

The photocatalytic activity of the powders is demonstrated in Fig. 8; (a) as concentration of methylene blue as a function of

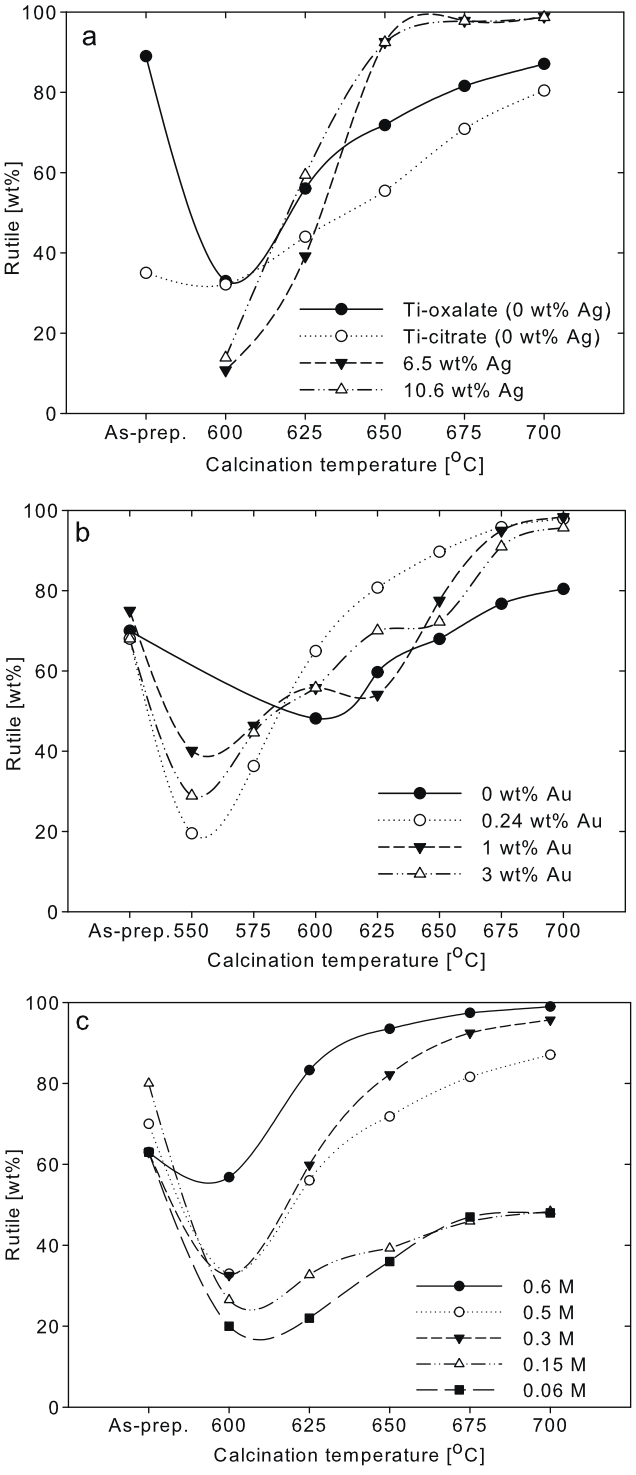


Fig. 6. Phase composition of spray pyrolysed $TiO_2$ photocatalyst as a function of calcination temperature. The wt% rutile is relative to (rutile + anatase) and measurement error is estimated to ±6%. (a) Powders in the Ag series including the oxalate sample, (b) powders in the Au series, and (c) powders in the concentration series.

UV-irradiation time for selected powders; (b) as reaction constants for the oxidation of methylene blue for selected samples as a function of calcination temperature. Powders were in contact with methylene blue solution prior to the UV-irradiation to remove the influence of adsorption. The concentration change

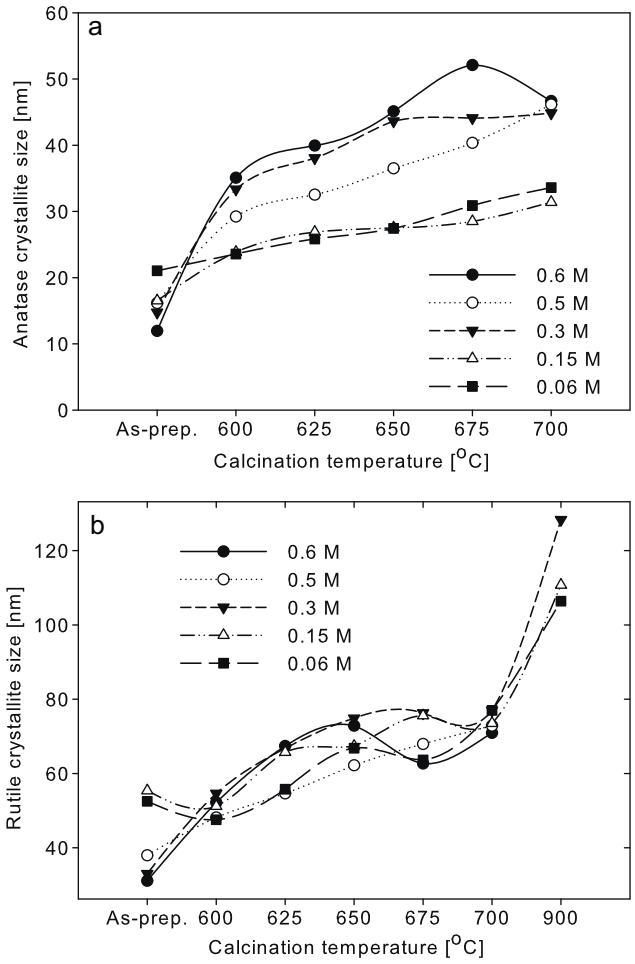


Fig. 7. Average crystallite size of spray pyrolysed $TiO_2$ photocatalysts vs. calcination temperature, here shown for the concentration series. Estimated measurement error is ±6%. (a) Anatase crystallite sizes, and (b) rutile crystallite sizes.

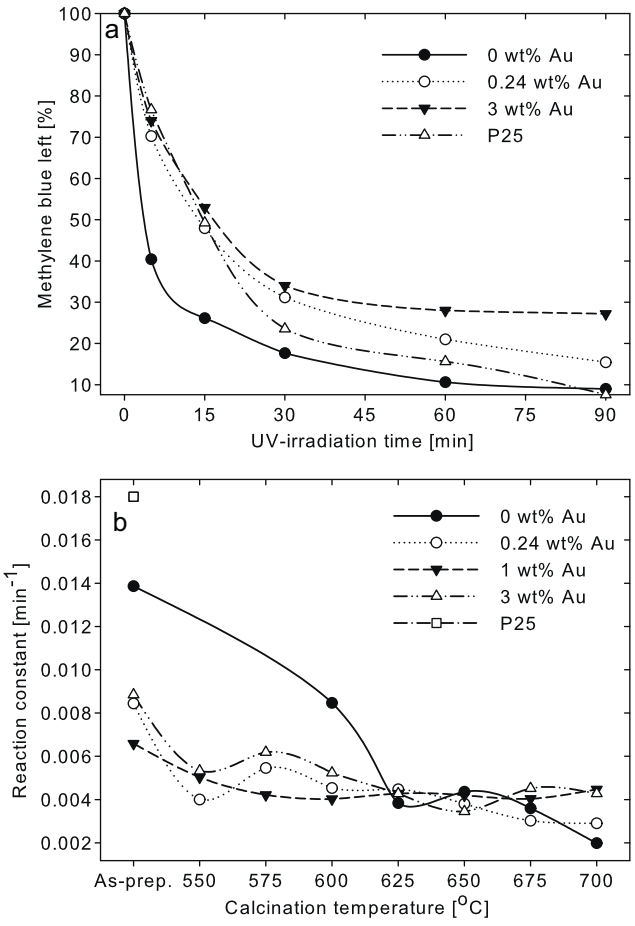


Fig. 8. (a) Methylene blue left after UV-irradiation by selected $TiO_2$ photocatalysts as a function of UV-irradiation time, and (b) first-order reaction constants for the oxidation of methylene blue by $TiO_2$ photocatalysts, measurement errors are estimated to be ±10%.

during the UV-irradiation is, thus, due to the photocatalytic oxidation. All the tested powders were photocatalytically active towards methylene blue oxidation, shown by the decreasing methylene blue concentration with time.

The most surprising result from the photocatalytic tests is the large photocatalytic activity of the as-prepared powders being mostly amorphous and containing ~30 wt% organic residuals. With or without metal incorporations their oxidative capacity is higher than for the calcined powders, as evident from Figs 8a and b. Compared to the commercial P25, the as-prepared $TiO_2$ sample from Ti–citrate oxidized methylene blue more rapidly (Fig. 8a), while its first order reaction constant is slightly smaller (Fig. 8b). Possible explanations of the high activity are a combination of large surface area, surface active groups[5] from organic residuals and photocatalytic mechanisms involving amorphous $TiO_2$, as previously suggested for P25.[8,22]

Powders calcined at low temperature (550–625 °C), especially the pure $TiO_2$ sample, exhibited higher first-order reaction constants than powders calcined at higher temperatures (650–700 °C). This observation may be explained by the higher amount of anatase in these low-temperature samples or by their larger surface area. No improvement of photocatalytic activity upon increased crystallite sizes could be found, probably due to the accompanied decrease in specific surface area and increased amount of rutile. The larger specific surface area of the powder produced from the oxalate precursor did not lead to a higher photocatalytic activity compared to the isopropoxide-based powders with smaller specific surface area.

As shown in Fig. 8b, no correlations between metal incorporation (type or amount) and photoactivity were found. This could be attributed to the relatively large size of the Ag and especially Au nanoparticles, resulting in metals acting as recombination centres on the metal–$TiO_2$ surface.[35] The critical metal size has previously been reported to be 10 nm.[18]

## 4. Conclusion

Spray pyrolysis is a suitable method for the large scale preparation of $TiO_2$ and metal-incorporated $TiO_2$ photocatalysts in one step. Proper conditions (preparation and calcination temperature) and precursor modifications (type and concentration) enabled preparation of photocatalysts with a large variety of crystallite sizes (12–120 nm), phase compositions (10–100% rutile) and metal loadings (up to 10.6 wt% Ag and 3 wt% Au). Incorporated metals were found homogeneously distributed

within the powders. The morphology consisted of hollow shells stable upon calcination and with decreasing size upon decreasing precursor concentration.

As-prepared photocatalysts with activity comparable to the commercial $TiO_2$ photocatalyst P25 were obtained. Photocatalysts calcined at lower temperatures (550–625 °C) exhibited slightly higher activities probably due to a larger amount of anatase than photocatalysts calcined at higher temperatures (650–700 °C). No effect of metal incorporations, specific surface area or crystallite size on photocatalytic activity was observed.

## Acknowledgements

TEM analyses were performed by Dr. Yingda Yu. The authors are grateful for funding from EEA in form of the grant PL0084 "NOMRemove".

## References

1. Fujishima A, Honda K. Electrochemical photolysis of water at a semiconductor electrode. *Nature (London)* 1972;**238**:37–8.
2. Chen X, Mao SS. Titanium dioxide nanomaterials: synthesis, properties, modifications, and applications. *Chem Rev* 2007;**107**:2891–959.
3. Lydakis-Simantiris N. Disinfection of spring water and secondary treated municipal wastewater by $TiO_2$ photocatalysis. *Desalination* 2010;**250**:351–5.
4. Liu S, Lim M, Fabris R, Chow C, Drikas M, Amal R. Comparison of photocatalytic degradation of natural organic matter in two Australian surface waters using multiple analytical techniques. *Org Geochem* 2010;**41**:124–9.
5. Mills A, Le Hunte S. An overview of semiconductor photocatalysis. *J Photochem Photobiol A* 1997;**108**:1–35.
6. Thomas AG, Flavell WR, Mallick AK, Kumarasinghe AR, Tsoutsou D, Khan N, et al. Comparison of the electronic structure of anatase and rutile $TiO_2$ single-crystal surfaces using resonant photoemission and X-ray absorption spectroscopy. *Phys Rev B: Condens Matter Mater Phys* 2007;**75**:12, 035105/1-035105/.
7. Hurum DC, Agrios AG, Gray KA, Rajh T, Thurnauer MC. Explaining the enhanced photocatalytic activity of Degussa P25 mixed-phase $TiO_2$ using EPR. *J Phys Chem B* 2003;**107**:4545–9.
8. Ohno T, Sarukawa K, Tokieda K, Matsumura M. Morphology of a $TiO_2$ photocatalyst (Degussa P 25) consisting of anatase and rutile crystalline phases. *J Catal* 2001;**203**:82–6.
9. Li H, Bian Z, Zhu J, Zhang D, Li G, Huo Y, et al. Mesoporous titania spheres with tunable chamber stucture and enhanced photocatalytic activity. *J Am Chem Soc* 2007;**129**:8406–7.
10. Lv K, Yu J, Deng K, Sun J, Zhao Y, Du D, et al. Synergistic effects of hollow structure and surface fluorination on the photocatalytic activity of titania. *J Hazard Mater* 2010;**173**:539–43.
11. Subramanian V, Wolf EE, Kamat PV. Influence of metal/metal ion concentration on the photocatalytic activity of $TiO_2$/gold composite nanoparticles. *Langmuir* 2003;**19**:469–74.
12. Jung KY, Park SB, Ihm S-K. Linear relationship between the crystallite size and the photoactivity of non-porous titania ranging from nanometer to micrometer size. *Appl Catal A* 2002;**224**:229–37.
13. Xin B, Jing L, Ren Z, Wang B, Fu H. Effects of simultaneously doped and deposited Ag on the photocatalytic activity and surface states of $TiO_2$. *J Phys Chem B* 2005;**109**:2805–9.
14. Iliev V, Tomova D, Bilyarska L, Eliyas A, Petrov L. Photocatalytic properties of $TiO_2$ modified with platinum and silver nanoparticles in the degradation of oxalic acid in aqueous solution. *Appl Catal B* 2006;**63**:266–71.
15. Seery MK, George R, Floris P, Pillai SC. Silver doped titanium dioxide nanomaterials for enhanced visible light photocatalysis. *J Photochem Photobiol A* 2007;**189**:258–63.
16. Chiarello GL, Selli E, Forni L. Photocatalytic hydrogen production over flame spray pyrolysis-synthesised $TiO_2$ and Au/$TiO_2$. *Appl Catal B* 2008;**84**:332–9.
17. Sakthivel S, Shankar MV, Palanichamy M, Arabindoo B, Bahnemann DW, Murugesan V. Enhancement of photocatalytic activity by metal deposition: characterisation and photonic efficiency of Pt, Au and Pd deposited on $TiO_2$ catalyst. *Water Res* 2004;**38**:3001–8.
18. Wang X, Mitchell DRG, Prince K, Atanacio AJ, Caruso RA. Gold nanoparticle incorporation into porous titania networks using an agarose gel templating technique for photocatalytic applications. *Chem Mater* 2008;**20**:3917–26.
19. Sathish Kumar PS, Sivakumar R, Anandan S, Madhavan J, Maruthamuthu P, Ashokkumar M. Photocatalytic degradation of Acid Red 88 using Au–$TiO_2$ nanoparticles in aqueous solutions. *Water Res* 2008;**42**:4878–84.
20. Iliev V, Tomova D, Todorovska R, Oliver D, Petrov L, Todorovsky D, et al. Photocatalytic properties of $TiO_2$ modified with gold nanoparticles in the degradation of oxalic acid in aqueous solution. *Appl Catal A* 2006;**313**:115–21.
21. Abrahams J, Davidson RS, Morrison CL. Optimization of the photocatalytic properties of titanium dioxide. *J Photochem* 1985;**29**:353–61.
22. Bickley RI, Gonzalez-Carreno T, Lees JS, Palmisano L, Tilley RJD. A structural investigation of titanium dioxide photocatalysts. *J Solid State Chem* 1991;**92**:178–90.
23. Chao HE, Yun YU, Xingfang HU, Larbot A. Effect of silver doping on the phase transformation and grain growth of sol–gel titania powder. *J Eur Ceram Soc* 2003;**23**:1457–64.
24. Debeila MA, Raphulu MC, Mokoena E, Avalos M, Petranovskii V, Coville NJ, et al. The effect of gold on the phase transitions of titania. *Mater Sci Eng A* 2005;**396**:61–9.
25. Kim C-S, Kwon I-M, Moon BK, Jeong JH, Choi B-C, Kim JH, et al. Synthesis and particle size effect on the phase transformation of nanocrystalline $TiO_2$. *Mater Sci Eng C* 2007;**27**:4.
26. Messing GL, Zhang SC, Jayanthi GV. Ceramic powder synthesis by spray pyrolysis. *J Am Ceram Soc* 1993;**76**:2707–26.
27. Simon C. Smart coatings based on nanosized capsules. *Eur Coat J* 2007;**2**:32–7.
28. Murugavel P. Sub-micrometre spherical particles of $TiO_2$, $ZrO_2$, and PZT by nebulized spray pyrolysis of metal-organic precursors. *J Mater Chem* 1997;**7**:1433–8.
29. Abdullah M, Iskandar F, Shibamoto S, Ogi T, Okuyama K. Preparation of oxide particles with ordered macropores by colloidal templating and spray pyrolysis. *Acta Mater* 2004;**52**:5151–6.
30. Deguchi S, Matsuda H, Hasatani M, Kobayashi N. Formation mechanism of $TiO_2$ fine particles by the spray pyrolysis method. *Drying Technol* 1994;**12**:577–91.
31. Lee J. Modification of titania particles by ultrasonic spray pyrolysis of colloid. *J MaterSci* 1999;**34**:4089–93.
32. Jokanovic V, Spasic AM, Uskokovic D. Designing of nanostructured hollow $TiO_2$ spheres obtained by ultrasonic spray pyrolysis. *J Colloid Interface Sci* 2004;**278**:342–52.
33. Wang W-N, Lenggoro IW, Terashi Y, Kim TO, Okuyama K. One-step synthesis of titanium oxide nanoparticles by spray pyrolysis of organic precursors. *Mater Sci Eng B* 2005;**123**:194–202.
34. Spurr RARA. Quantitative analysis of anatase-rutile mixtures with an X-ray diffractometer. *Anal Chem* 1957;**29**:760–2.
35. Kamat PV. Photoinduced transformations in semiconductor-metal nanocomposite assemblies. *Pure Appl Chem* 2002;**74**:1693–706.